Department of Physics: MSc in Fusion Energy

ICF Data Laboratory

Pre-reading : NOVA Inertial Confinement Fusion Experiments

Aims

Through the analysis of this data you have the opportunity to gain first hand experience of working with and appreciating the limitations of inertial confinement fusion data. By taking this laboratory you can develop familiarity with x-ray imaging and spectroscopic techniques. These techniques are applicable to many laser-plasma experiments and software tools and procedures to extract quantitative information from the data are quite general.

- Safety hazards and precautions:
  - None: Appropriate use of display screen equipment (see http://www.hse.gov.uk/pubns/indg36.pdf)
- Experimental Objectives:
  - To be aware of what can be learned from x-ray emission data.
  - To understand how to apply interpolation and curve fitting to infer quantitative information.
  - To apply the type of corrections necessary to extract and interpret quantitative information.
  - To refer to published literature and extract data for use in analysis.
- Learning Outcomes:
  - To understand how to handle, correct and analyse x-ray imaging and spectroscopic data.
  - To be competent in using a number of software tools.
  - To understand limitations on information extracted from measurements.
  - To appreciate the reliance on published literature.
- Script Updated: October 2017

1 The Task

This experiment is about analysing x-ray measurements taken from an indirectly driven inertial confinement fusion (ICF) experiment. The data you will analyse consists of time-resolved x-ray self-emission pinhole images recorded on a gated x-ray imager (GXI) and x-ray spectra recorded on a streak camera (SSC). By the end of this experiment you should have an estimate of the imploded target density. X-ray imaging and spectroscopy are techniques commonly applied to a wide variety of laser-plasma experiments. The techniques and resources you will use in this laboratory are generic and suitable for analysing data from many instruments and experiments, and these are not limited to ICF.

2 The Experiment

The measurements where taken on the ten beam Nova laser facility at the Lawrence Livermore National Facility in the mid 1990s. Figure 1 shows an illustration of the experiment. This illustration includes four of the ten laser beams, the hohlraum, capsule, and the two diagnostics of interest. A key reference is Lindl [1], this article presents a thorough review of indirectly driven ICF, and the text by Atzeni and Meyer-ter-vehn [2] cover all aspects for inertial fusion. The success of ICF depends on the ability to maintain a high level of drive uniformity throughout the implosion; drive uniformity is one advantage of indirect drive approach.

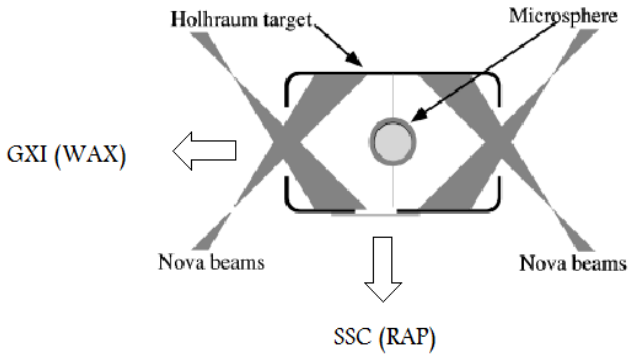

Figure 1: This diagram illustrates a Nova implosion experiment. This includes a scale-1 hohlraum, with two of the 5 Nova beams entering the west (left) and east (right) laser entrance hole (LEH) a deuterium filled capsule. The GXI images the implosion through the west LEH, the SSC records argon emission spectra through a diagnostic hole on the south side of the hohlraum.

Lasers irradiate the inner walls of a mm-scale gold cavity, or hohlraum, at intensities of 10^{15} W/cm^2, the intensity-wavelength-squared product of ~10^{14} W.cm^{-2}.μm^2 is sufficiently low to prevent the excitation of parametric instabilities. Ten beams deliver approximately 20 kJ of energy to the hohlraum creating radiation temperatures approaching 200 eV. The radiation field in the hohlraum drives the compression of a sub-mm diameter deuterium-filled plastic capsule suspended at the centre of the hohlraum. The compression occurs as the radiation heats the outer plastic layer, or ablator, of the capsule. The rapid expansion of the ablator into the hohlraum and momentum conservation drives the compression of the capsule interior. As the capsule compresses an array of diagnostics record the x-ray, fast particle and neutron emission. Neutron production results from

$$D + D \rightarrow \begin{array}{ll} T(1.01MeV) + p(3.02MeV) & 50\% \\ He^3(0.82MeV) + n(2.45MeV) & 50\% \end{array} \quad (1)$$

This script focuses on the x-ray pinhole (GXI) and x-ray spectroscopy (SSC) measurements. The experiments (laser beam, hohlraum and capsule) were designed to approach one-dimensional performance rather than high neutron yield.

3 The Target

The target consists of a hohlraum and capsule as illustrated in Figures 1, 2 and Table 1 summarises the target design parameters. The capsule consists of a deuterium filled 440 µm diameter plastic microsphere placed in the centre of a 20 µm thick gold hohlraum. Argon, added in trace amounts (see Table 1) as a diagnostic dopant, enables x-ray emission imaging and spectroscopy of the imploding core.

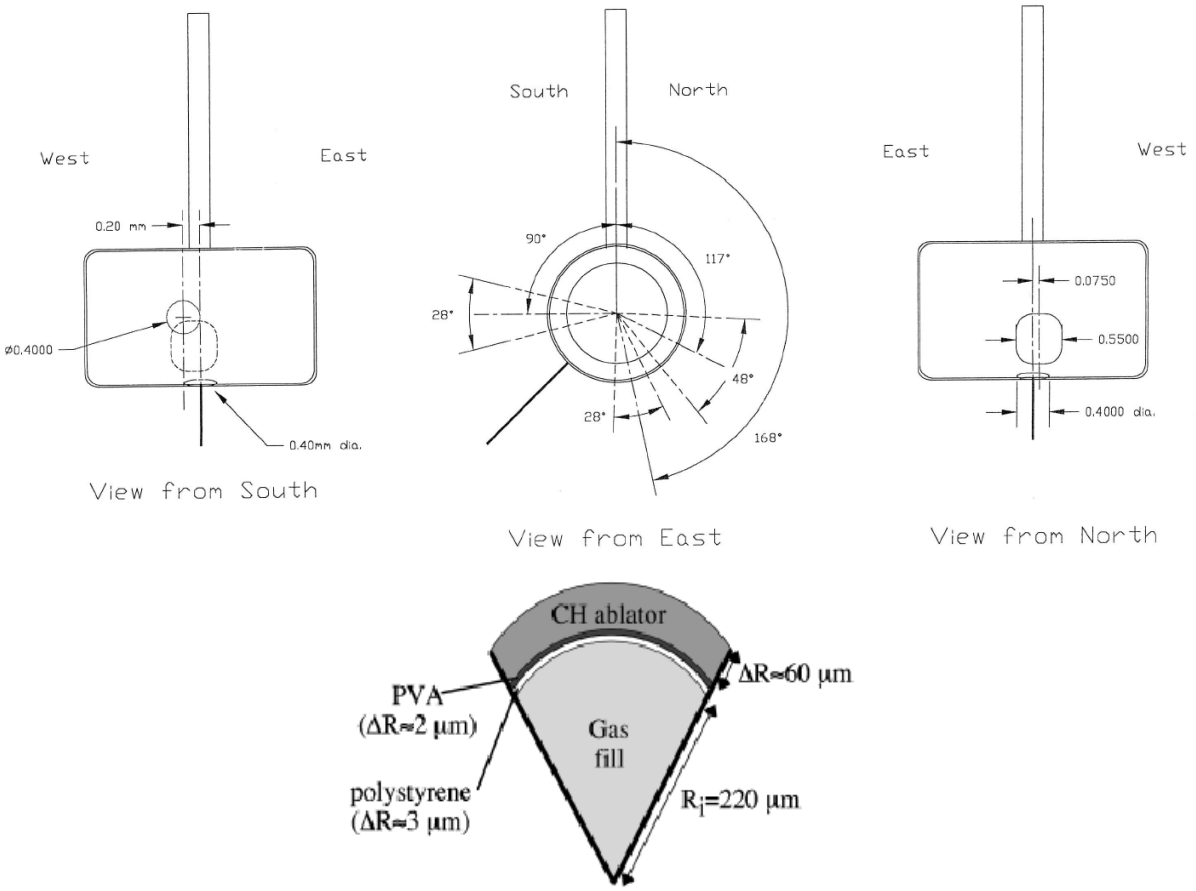

Figure 2: a) This drawing of a scaling-1 hohlraum shows the positioning of the diagnostic holes to enable line-of-sight between the capsule and diagnostic equipment. b) This sketch shows the capsule construction. The capsule sits at the centre of a scale-1 hohlraum (Figure 1). Significant effort is required to ensure that the capsule is spherical and with minimal surface perturbations. The capsule is held in the centre of the hohlraum using a 40 nm thick plastic web.

Hohlraum		Capsule	
Length	2.55 mm	Inner diameter	440 µm
Diameter	1.60 mm	Wall (inner) PS	3 µm
Laser entrance hole	0.80 mm	PVA (sealant)	2 µm
Diagnostic holes	3	CH (ablator)	55 µm
Diagnostic hole cover	Be 12 µm	Gas fill (core)	D_2(50 atm) Ar (0.1 atm)

Table 1: This table summarises the hohlraum and capsule design parameters.

The hohlraum design allows access for four diagnostics to record keV energy x-rays emission from highly ionised argon. In this laboratory you have the opportunity to analyse measurements from a GXI (or West Axial X-ray imager, WAX) that records emission through the west laser entrance hole (LEH), and a survey crystal spectrometer (RAP) coupled to an SSC that records K-shell emission from argon through a laser diagnostic hole in the south side of the hohlraum. The positions of these instruments are shown in Figure 1. In addition, a second GXI records

emission through a diagnostic hole on the south of the hohlraum, and a high-resolution crystal spectrometer records argon He-β emission from below and to the north of the hohlraum. The diagnostic holes are covered with beryllium in an attempt to maintain the hohlraum albedo and drive uniformity.

4 The Diagnostic Instrumentation

Two particular challenges of inertial confinement fusion, and most other laser plasma experiments, are the short duration of an experiment and the small spatial scales on which the physics occurs. The high energy densities result in plasmas that tend to be extremely bright emitters of x-ray radiation. Ideally, a measurement should resolve target dynamics with both temporal and spatial information. The two approaches considered here are the gated x-ray imager (GXI) and a streak camera (SSC) and, in part, achieve these ideals.

a) The GXI pinhole imaging

A GXI is a gated, time-resolving two spatial dimension imaging instrument (see Refs [3] & [4]). The instrument can achieve temporal resolution below 100 ps. The illustration of a GXI in Figure 3 shows the instrument recording x-ray radiation through an array of pinholes. The system operates as a pinhole camera, and x-rays that pass through a pinhole cast an image of the radiation source on a micro-channel plate (MCP). Radiation incident on the MCP produce photo-electrons. On placing a voltage across the MCP some of these photo-electrons accelerate and cause an electron avalanche as they hit the sides of the holes (or micro-channels) in the plate. This greatly amplifies the photo-electron signal. On exiting the MCP, the electrons strike a phosphor screen producing light. A measurement is made by recording this light on film or CCD. By changing the voltage across the MCP very quickly it is possible to gate (that is rapidly turn on and off) the accelerating voltage to produce a time resolved image. Optical analogues of the GXI are referred to as gated optical imagers (GOI).

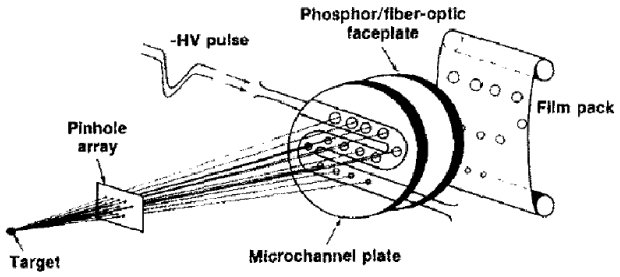

Figure 3: Multiframe imaging uses a pinhole array a single meander microstrip on a micro-channel plate (MCP) to amplify photo-electron production, a phosphor plate to convert the MCP signal into light. The light is recorded on film or CCD camera. Image is taken from Ref 1. The MCP, phosphor system is referred to as a GXI.

The GXI or West-Axial-Imager (WAX) in Figure 3 consists of single meander strip of gold, the photocathode, with twelve 15 μm diameter pinholes casting images on the strip. The instrument is filtered with 380 μm of beryllium. This instrument images the target through the west LEH with a magnification of x3.5.

b) X-ray streak cameras and the SSC

Streak cameras are used to record radiation, x-ray or optical, with very high temporal resolution (~1ps or better). Streak cameras used on Nova where referred to as SSCs [5]. In most cases radiation from a target falls on a slit at the front of the camera, a photocathode converts this radiation image at the slit into electrons. A grid accelerates the electrons in to an electrostatic focusing system to preserve the image, and then between a set of deflection plates. The exceptional time resolution comes from ramping a voltage (using nonlinear avalanche electronics)

across the plates and sweeping the electrons across a phosphor, this is similar to the raster on old-style cathode ray tubes.

Changes in radiation intensity at the photocathode result in changes of light emission from the phosphor. Film or CCD cameras record the phosphor emission. The result is a two-dimensional image. Time is represented along the axis perpendicular to the slit, whilst spatial (or spectral) information is along the slit. The slit limits spatial (spectral) resolution to one dimension and to only a section of the radiation source, or spatially integrates the sources of small spatial extent.

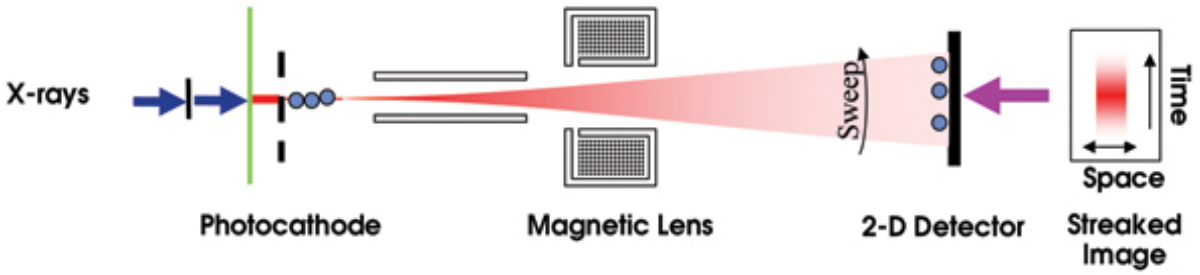

Figure 4: Streak cameras use a deflection plate system to deliver exceptional time resolution. It is possible to achieve time resolutions < 1 ps with specially configured streak cameras. The final result is a two-dimensional streaked image with time in one dimension and spatial or spectral information in the other dimension.

c) Argon K-shell spectroscopy

The front of the SSC was fitted with a crystal spectrometer snout [6]. The crystal is 100 mm long, 20 mm wide rubidium acid phthalate ($RbHC_8H_4O_4$) crystal. The accepted name for this crystal is RAP. The RAP (100) planes have a 2d-spacing of 26.121 Å [7]. A 50 mm thick tantalum shield blocks direct line-of-sight x-rays from the target hitting the SSC and a series of apertures in 1.5 mm thick brass plates restricts x-ray illumination to the crystal surface and suppresses x-ray scatter within the snout. In Nova the distance between the SSC slit and target chamber centre was 0.482 m. The 100 mm long crystal, housed in the snout, was centred 0.247 m from target chamber centre and 33 mm off the direct line-of-sight between the target and the centre of the SSC slit. The spectral resolution is affected by the SSC spatial resolution.

The resonance transition energies of Ly-like (Ar^{17+}) and He-like (Ar^{16+}) argon are shown in Table 2, and indicated on Figure 5. You will need to refer to these in Part III of the laboratory.

Ly-like term	$2P_{1/2}$	$2P_{3/2}$	$3P_{1/2}$	$3P_{3/2}$	$4P_{1/2}$	$4P_{3/2}$
Symbol	Ly-α(*)	Ly-α	Ly-β(*)	Ly-β	Ly-γ(*)	Ly-γ(*)
Energy (eV)	3318.1	3322.9	3934.2	3935.6	4149.6	4150.2

He-like term	2^3P_1	2^1P_1	3^3P_1	3^1P_1	4^3P_1	4^1P_1
Symbol	He-α	He-α	He-β(*)	He-β	He-γ(*)	He-γ
Energy (eV)	3123.4	3139.3	3679.3	3683.7	3872.9	3874.4

Table 2: Energies of transitions to the ground state of Ly- and He-like argon, taken from Scofield [8], more detail is available via the NIST ADS database [9] and the GENIE portal [10]. The transitions marked with a (*) are weak, and so you won't be able to identify them in your data.

5 The Data

The GXI pinhole and SSC with RAP spectrometer data you are asked to analyse are shown in Figure 5. This data was recorded on Kodak TMAX3200 film and has been digitised at 12-bit and 60-μm spatial resolution and corrected for film response to exposure.

The GXI(WAX) camera was aligned to record the capsule x-ray emission above 3 keV through the west LEH, viewing along the axis of the hohlraum target and was equipped with a single continuous meander strip recording 12 images at a magnification of 3.5 through 15-μm-diameter pinholes [11]. The camera was filtered with 600 μm of beryllium. The initial images top-left in Figure 5a show x-ray emission from the hohlraum LEH heated by laser irradiation.

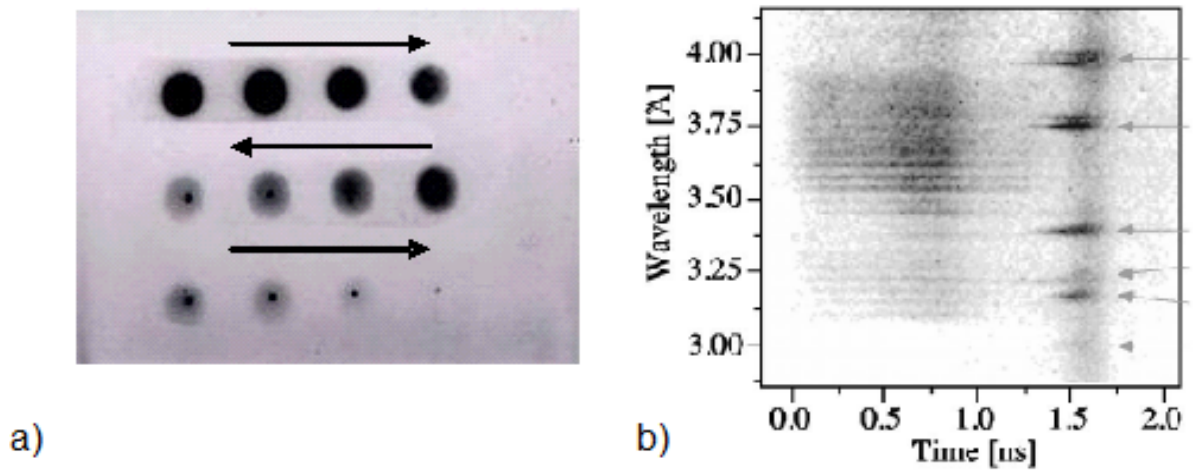

Figure 5: a) GXI(WAX) images showing x-ray emission >3 keV from the LEH at early times (< 1 ns) at the top-left and the imploding capsule core at later times. The arrows indicate time along the strip. Inter-image timing is 200 ps. b) A SSC(RAP) time resolved spectral measurement between 2.7–4.2 Å of the implosion. Strong gold M-band emission occurs to ~ 1 ns, at >1.2 ns argon K-shell emission from the capsule core dominates.

As time progresses beyond 1 ns the emission from the LEH weakens and emission from the imploding capsule at the centre of the LEH increases. As the implosion continues the capsule core reduces in size, i.e. it compresses, after peak compression the core disassembles and cools. One of the main applications of gated imaging is that it allows us a means of checking the accuracy of hydrodynamic code predictions and the uniformity of the compression.

The SSC was configured with a low-spectral-resolution RAP survey spectrometer to record the Ar K-shell emission in the spectral range of 2.7 - 4.2 Å through a 390 - 500 μm^2 diagnostic hole centred at $\varphi = 90°$ and $\theta = 104°$. Where the hohlraum target axis is define as $\varphi = 90°$ and $\theta = 0°$, with φ the polar angle and θ the azimuthal angle. The temporal resolution of the streak camera is determined from the sweep speed, the slit width, the camera magnification, and the spatial resolution. The SSC uses a caesium iodide (CsI) photocathode [12], [13] has a magnification of x1.24 and a sweep speed of 63 ps/mm. A slit of width 0.25 mm is placed in front of the photocathode to improve the temporal resolution. The SSC spatial resolution was measured as 150 μm in the central 15-20 mm of the camera, deteriorating to 400 μm towards the edges [14]. The cameras were filtered with a total of 385 μm of beryllium.

The SSC data in Figure 5b shows bright gold M-band emission for the first nanosecond while the laser irradiates the hohlraum target interior. The M-band emission decays rapidly as the laser turns off. By $t \sim 1.25ns$ Ar K-shell emission is observed and the K-shell emission intensity increases as the implosion proceeds. The Ar He-β emission intensity peaks at 1.6 ns, remains high for a further 0.1 ns, and then falls rapidly; after 1.8 ns the continuum is dominant and the Ar K-shell is not visible. Between $1.5ns \lesssim t \lesssim 1.75ns$ Ar K-shell spectra are superimposed on bright continuum emission from the converging shell.

References

[1] John D. Lindl et al., The physics basis for ignition using indirect-drive targets on the National Ignition Facility, Phys. Plasmas 11, 339 (2004)

[2] S. Atzeni & J. Meyer-ter-vehn, The Physics of Inertial Fusion, Clarendon Press (2004)

[3] D. K Bradley et al, High-speed gated x-ray imaging for ICF target experiments, Rev. Sci. Instrum. 63, 4813 (1992)

[4] http://www.kentech.co.uk/PDF/ENEA_SLIX.pdf

[5] D. H. Kalantar et al., Characterization of X-ray Streak Cameras for Use on Nova, UCRL-JC-12377t5-Rev 1 (1996)

[6] B. A. Hammel et al., K- and L-shell x-ray spectroscopy of indirectly driven implosions, Rev. Sci. Instrum. 63, 5017 (1992)

[7] Centre for X-ray Optics, X-ray data booklet, http://xdb.lbl.gov/

[8] J. H. Scofield, Energies of hydrogen and helium like ions for Z's from 6 to 54, UCID – 16848 (1975)

[9] http://physics.nist.gov/PhysRefData/ASD/index.html

[10] http://www-amdis.iaea.org/GENIE/

[11] E. M. Campbell, Laser Part. Beams 9, 209 (1991)

[12] B. L. Henke eta al ., The characterization of x-ray photocathodes in the 0.1–10-keV photon energy region, J. Appl. Phys. 52, 1509 (1981)

[13] B. L. Henke et al., Soft-x-ray-induced secondary-electron emission from semiconductors and insulators: Models and measurements, Phys. Rev. B 19, 3004 (1979)

[14] BL Henke, EM Gullikson, JC Davis, Atomic Data and Nuclear Tables, 54, 181-342 (1993)

[15] K. Premaratne, E. R. Dietz, and B. L. Henke, Nucl. Instrum. Methods Phys. Res. 207, 467 (1983); B. L. Henke, J. P. Knauer, and K. Premaratne, J. Appl. Phys. 52, 1509 (1981); B. L. Henke, in Low Energy X-Ray Diagnostics, edited by David T. Attwood and Burton L. Henke, AIP Conf. Proc. 75 (AIP, New York, 1981), p. 146.

[16] H. R. Griem, Plasma Spectroscopy, McGraw-Hill (1964)

[17] H. R. Griem, Principles of Plasma Spectroscopy, CUP (1997)

[18] http://nlte.nist.gov/FLY/

[19] H. K. Chung et al., FLYCHK: Generalized population kinetics and spectral model for rapid spectroscopic analysis for all elements, High Energy Density Physics, 1, 3 (2005)

[20] I. H. Hutchinson, Principles of Plasma Diagnostics, 2nd ed., CUP (2002)

[21] B. A. Hammel, C. J. Keane, M. D. Cable, D. R. Kania, J. D. Kilkenny, R. W. Lee, and R. Pasha, X-ray spectroscopic measurements of high densities and temperatures from indirectly driven inertial confinement fusion capsules, Phys. Rev. Lett. 70, 1263 (1993)